

Adaptive Real-Time Multi-Loss Function Optimization Using Dynamic Memory Fusion Framework: A Case Study on Breast Cancer Segmentation

Amin Golnari  ^{a,*}, Mostafa Diba  ^a

^a*Faculty of Electrical & Robotics, Shahrood University of Technology, Shahrood, Iran*

Abstract

Deep learning has proven to be a highly effective tool for a wide range of applications, significantly when leveraging the power of multi-loss functions to optimize performance on multiple criteria simultaneously. However, optimal selection and weighting loss functions in deep learning tasks can significantly influence model performance, yet manual tuning of these functions is often inefficient and inflexible. We propose a novel framework called dynamic memory fusion for adaptive multi-loss function penalizing in real-time to address this. This framework leverages historical loss values data to dynamically adjust the weighting of multiple loss functions throughout the training process. Additionally, this framework integrates an auxiliary loss function to enhance model performance in the early stages. To further research horizons, we introduce the class-balanced dice loss function, designed to address class imbalance by prioritizing underrepresented classes. Experiments on breast ultrasound datasets demonstrate that the framework improves segmentation performance across various metrics. These results demonstrate the effectiveness of our proposed framework in ensuring that the model dynamically adjusts its focus to prioritize the most relevant criteria, leading to improved performance in evolving environments. The source code for our proposed methodology is publicly available on GitHub.

Keywords: Multi-Loss Optimization, Penalizing Loss Functions, Class-Balanced Dice Loss, Medical Imaging, Breast Cancer Segmentation

1. Introduction

In deep learning, the strategic selection, combination, and dynamic weighting of loss functions are crucial for optimizing performance across various tasks. This is particularly important when dealing with challenges like class imbalance, boundary

^{*}*Corresponding author*

Email addresses: amingolnarii@gmail.com (Amin Golnari )m.diba@shahroodut.ac.ir (Mostafa Diba )

precision, and feature learning. Deep learning models can achieve superior results in various domains by carefully considering these factors and employing appropriate loss functions. In GBE-Net [1], the combination of cross-entropy and dice loss is shown to enhance segmentation accuracy, particularly in preserving the boundaries of lesions. Similarly, MFMSNet integrates dice and binary cross-entropy losses to handle class imbalance while refining tumor edges through multi-scale fusion [2].

In complex models, dynamically adjusting the weights of individual loss functions during training is essential for effectively balancing them. Approaches like SoftAdapt dynamically adjust the weights of loss components, such as mean squared error (MSE) and Kullback-Leibler (KL) divergence, to optimize tasks like autoencoders and variational autoencoders. This ensures a more balanced learning process, preventing the model from overly focusing on any criterion. [3]. The dynamically weighted balanced (DWB) loss proposed by Ruwani et al. [4] improves accuracy in class-imbalanced datasets by adjusting weights based on class frequency and prediction difficulty. These dynamic weighting strategies are crucial in applications where class imbalance significantly impacts model performance.

Another example of an adaptive loss function application is found in unsupervised image segmentation. Guermazi et al. [5] developed a dynamically weighted loss function that balances feature similarity and spatial continuity during training. The balance is automatically adapted based on cluster predictions, allowing more accurate and semantically meaningful segmentations. Similar dynamic approaches are applied in multiorgan segmentation, where Song et al. [6] introduced a dynamic loss weighting algorithm that adjusts the weight assigned to each organ based on its learning difficulty, ensuring more consistent performance across organs with varying sizes and complexities.

The need for customized composite loss functions also extends to image fusion and classification tasks. Research such as FuseFormer [7] and S2F-Net [8] have introduced loss functions that balance pixel-level accuracy and structural similarity to ensure quality fusion results in infrared and visible image fusion. Finger vein recognition (FVR) also benefits from composite loss functions, where combining cosine softmax and triplet loss improves feature learning, generalization, and robustness [9]. In the context of ultrasound diagnosis systems, combining class activation mapping (CAM)-based loss and quantitative ultrasound (QUS)-based loss using fixed weights improves classification accuracy by enhancing lesion discrimination [10].

Meta-learning techniques have also been applied to dynamic loss weighting, as shown by Jiang et al. [11], who proposed a meta-learning loss function that adapts to label noise and class imbalance in biased datasets by dynamically adjusting loss weights based on learned margins. These approaches demonstrate the effectiveness of both composite and dynamic loss functions in enhancing performance across a wide range of deep learning applications.

In this research, we introduce the dynamic memory fusion (DMF) framework, which builds upon these advancements by dynamically adjusting the weights of multiple base loss functions during training. Unlike fixed-weight approaches, the DMF

framework leverages historical loss data to dynamically adjust the weighting of individual loss functions in real time. This adaptive approach ensures a balanced focus on different aspects of the learning task, preventing the model from becoming overly biased towards any single component. Our framework draws inspiration from previous studies on composite loss functions and dynamic weighting, offering a solution for multi-loss function optimization in deep learning.

2. Background

Deep learning tasks, especially in the domains of segmentation, classification, and regression, have increasingly relied on composite and dynamically weighted loss functions to address challenges such as class imbalance, boundary precision, and feature learning. A growing body of research has explored how combining multiple loss functions and dynamically adjusting their weights can lead to more effective optimization, particularly for tasks requiring complex decisions at multiple scales and resolutions.

In medical imaging, composite loss functions have become popular in improving segmentation accuracy. Jesson et al. [12] introduced a novel approach to brain tumor segmentation using a 3D fully connected network (FCN) with a multi-scale loss function. This composite loss ensures learning at different spatial resolutions by comparing predictions with down-sampled ground truth, addressing class imbalance through a curriculum sample weighting strategy. Similarly, Sharifzadeh et al. [13] developed an adaptive mixed loss function for ultrasound imaging, gradually shifting from more straightforward B-mode data to more complex RF data. This progressive approach improves reconstruction accuracy and avoids local minima during training, resembling curriculum learning techniques.

Dynamic and composite loss functions have also been employed in diverse fields beyond medical imaging. For example, Lv et al. [14] introduced SSDFusion, which leverages a composite loss combining fusion and segmentation losses to fuse infrared and visible images effectively while maintaining semantic accuracy. Similarly, Gao et al. [15] enhanced face recognition performance by fusing multiple loss functions automatically, learning the optimal balance between intra-class compactness and inter-class separation. Moreover, attention-based models, such as the attention-gate medical transformer (AGMT) for ultrasound image segmentation, incorporate specialized loss functions like the average radial derivative increment (Δ ARD) to improve shape feature detection, while other methods like δ ARD further enhance the sensitivity to contours and regions in low-contrast medical images [16, 17].

Adaptive loss functions have proven effective in segmentation tasks where visual detail is crucial. Chao et al. [18] introduced an adaptive composite loss function for a multi-field-of-view (FoV) visual saliency model in 360° image processing. This method dynamically adjusts the weights of Kullback-Leibler divergence (KLD), normalized scanpath saliency (NSS), and linear correlation coefficient (CC) based on their standard deviations during training. By doing so, the model optimizes performance by balancing key saliency features. Similarly, B et al. [19] developed a deep

learning model for breast lesion segmentation in ultrasound images using a composite loss that combines binary cross-entropy (BCE) and boundary loss, demonstrating the efficacy of composite loss functions in medical image analysis.

Dynamic loss weighting methods have also been introduced to tackle imbalanced datasets and optimize neural network training. Mang et al. [20] presented DYNNAWEIL, a dynamic weighted loss function for solving partial differential equations (PDEs) on imbalanced data. By adjusting the weights of the loss based on historical errors during training, DYNNAWEIL improves prediction accuracy in regions with high errors. Similarly, Lu et al. [21] introduced dynamic weighted cross entropy (DWCE) for semantic segmentation, where cross-entropy loss is dynamically weighted based on class proportion to handle class imbalance effectively. Additionally, Maldonado et al. [22] introduce an adaptive loss function based on ordered weighted averaging (OWA) operators, dynamically adjusting class weights to handle class imbalance and noise, improving classification performance over traditional methods like focal loss and cross-entropy.

Dynamic loss weighting also finds applications in sentiment classification, as demonstrated by Runda et al. [23], who introduced a model that adjusts the weights of loss functions based on class prediction error rates, ensuring stable training even in imbalanced datasets. A problem also addressed by Roy et al. [24] in their margin-aware adaptive-weighted loss (MAAW), which enhances intraclass compactness and interclass separability by dynamically adjusting weights for hard-to-train samples using confidence scores.

In tasks requiring the balance of multiple cost functions, novel dynamic loss weighting strategies have shown significant performance improvements. Groenendijk et al. [25] introduced CoV-weighting, a multi-loss weighting strategy for single-task learning problems such as depth estimation and semantic segmentation. By utilizing the coefficient of variation, CoV-weighting dynamically adjusts the weights of loss functions, eliminating the need for manual weight tuning and grid searches. Ocampo et al. [26] extended this idea by introducing an adaptive loss weighting approach for machine learning interatomic potentials (ML-IAPs). Using the SoftAdapt algorithm, this method recalibrates the contribution of each loss component based on their loss values, ensuring that no single component dominates the training process.

Xiang et al. [27] introduced lbPINNs, a self-adaptive loss-balanced method for physics-informed neural networks (PINNs). This model adaptively assigns weights to multiple loss terms during training, optimizing them at each epoch through Gaussian probabilistic models. Barron [28] further extended this concept by proposing a generalized adaptive robust loss function that unifies several well-known loss functions, such as Cauchy and Charbonnier, enabling automatic adjustment during training for improved performance across a range of computer vision tasks.

These studies underscore the importance of combining loss functions and dynamically adjusting their weights to address diverse challenges across deep learning applications. Whether handling class imbalance, ensuring boundary precision, or improving segmentation accuracy, dynamic and composite loss functions provide robust

solutions for optimizing neural networks in various tasks.

3. Methodology

Manually selecting and weighting multiple loss functions in deep learning can be a complex task, as the relative importance of each cost function may evolve throughout the training process. A fixed weight assignment is often inadequate, as it fails to account for the dynamic nature of learning, where different components may require varying levels of focus at various stages. A more logical approach is to implement a system that can dynamically adjust the weights of each loss function based on their real-time contributions to the model's overall performance. This framework adjusts weights during the training process in real-time, running in parallel with model training. The computational overhead is minimal, requiring only the storage of a subset of historical loss function values in small arrays. Consequently, memory consumption remains low, ensuring computational efficiency even for complex tasks. This adaptive weighting maintains a balanced and responsive training process, leading to more effective optimization.

We introduce the DMF framework for adaptive loss optimization to address the challenges inherent in deep learning tasks involving multiple loss functions. This section details the loss function's components, strategies for weight adjustment, the integration of auxiliary losses, and the computational considerations involved.

3.1. Dynamic Memory Fusion Framework

The primary objective of the proposed framework is to minimize a DMF loss function, denoted as \mathcal{L} , which integrates multiple base loss functions with an auxiliary loss that addresses specific task-related challenges, such as improving generalization or mitigating bias. The total loss function is defined as:

$$\mathcal{L}(y, \hat{y}) = \sum_{i=1}^N w_i \mathcal{L}_i(y, \hat{y}) + \gamma(t) \mathcal{L}_a(y, \hat{y}) \quad (1)$$

where y and \hat{y} refer to ground truth and predicted labels, respectively; N represents the number of base loss functions, \mathcal{L}_i are the individual loss functions, w_i are adaptive weights dynamically adjust based on the historical data of each loss function, \mathcal{L}_a denotes the auxiliary loss, which can be any task-specific function critical in early training stages, γ is a scaling factor controlling the contribution of the auxiliary loss, and t indicates the current training step.

This formulation allows the model to adaptively prioritize different loss functions throughout the training process, ensuring a balanced and optimized performance while also incorporating essential task-specific considerations through the auxiliary loss function.

3.2. Regularizing Loss Function

The auxiliary loss function, denoted as \mathcal{L}_a , is integral to guiding the model during the early stages of training by incorporating additional objectives crucial for the learning process. The definition of the auxiliary loss is flexible and can be tailored to the specific task and objectives at hand. The auxiliary loss is typically designed to emphasize aspects of the model that require special attention during training, particularly in the early phases when the model is still learning foundational patterns in the data. To ensure that the influence of the auxiliary loss is most potent during these initial stages and diminishes as training progresses, it is scaled by an exponential decay factor γ , which is defined as:

$$\gamma(t) = \gamma_0 e^{-\tau t} \quad (2)$$

where γ_0 represents the initial weight of the auxiliary loss, and τ is the decay rate. This scaling mechanism allows the auxiliary loss to influence the model during the early training steps, guiding the learning process toward specific goals. As the training progresses and the model converges, the primary loss function gradually takes precedence, allowing for a balanced and comprehensive optimization process.

4. Dynamic Weight Adjustment with Memory

The proposed framework's dynamic adjustment of weights w_i for each loss function is driven by historical loss-value data, referred to as memory. This section details the role of memory in the weight adjustment process and its impact on optimization, as well as the mechanism and strategies of the DMF for weight adjustment.

4.1. Memory Mechanism

In the DMF framework, memory plays a pivotal role in adapting the weights of the loss functions over time. Each loss function maintains a record of its historical loss values, which are utilized to compute statistical measures that guide the adjustment of weights. The DMF framework employs three memory-based weighting strategies: variance-based weighting, median absolute deviation (MAD)-based weighting, and Bayesian-based weighting.

4.2. Variance-Based Weighting

The variance-based weighting approach adjusts the weight w_i of each loss function according to the variance of its loss history \mathcal{H}_i . The variance is calculated as follows:

$$Var(\mathcal{H}_i) = \frac{1}{|\mathcal{H}_i|} \sum_{k=1}^{|\mathcal{H}_i|} \left(\mathcal{H}_i^{(k)} - \bar{\mathcal{H}}_i \right)^2, \quad (3)$$

where $|\mathcal{H}_i|$ is the size of the loss history for the i -th loss function, $\mathcal{H}_i^{(k)}$ denotes the k -th value in the loss history, and $\bar{\mathcal{H}}_i$ represents the mean of the loss history.

The weight w_i with N base loss functions is then normalized to ensure a balanced distribution:

$$w_i = \frac{Var(\mathcal{H}_i)}{\sum_{j=1}^N Var(\mathcal{H}_j)}, \quad (4)$$

This normalization ensures that loss functions exhibiting higher variance are assigned greater weight, reflecting their increased contribution to the overall optimization process.

4.3. MAD-Based Weighting

The MAD-based weighting approach offers robustness against outliers by utilizing the median absolute deviation from the median of the loss history. The MAD for the i -th loss function is computed as:

$$MAD(\mathcal{H}_i) = median \left(\left| \mathcal{H}_i^{(k)} - median(\mathcal{H}_i) \right| \right) \quad (5)$$

where $median(\cdot)$ represents the median operation. The weight w_i for N base loss functions is then determined by:

$$w_i = \frac{(MAD(\mathcal{H}_i))^{-1}}{\sum_{j=1}^N (MAD(\mathcal{H}_j))^{-1}} \quad (6)$$

This approach favors loss functions with lower deviations from their median values, ensuring that more stable loss functions are weighted more heavily.

4.4. Bayesian-Based Weighting

The Bayesian-based weighting strategy updates weights based on likelihoods derived from the MAD values. The likelihood for the i -th loss function is given by:

$$p(MAD_i|data) \propto \frac{1}{MAD(\mathcal{H}_i)} \quad (7)$$

The posterior distribution for the weight w_i for N base loss functions is then calculated as:

$$w_i = \frac{p(MAD_i|data) \cdot p_i}{\sum_{j=1}^N p(MAD_j|data) \cdot p_j} \quad (8)$$

where p_i represents the prior probability for the i -th loss function. This approach integrates prior knowledge with observed data, allowing for a more informed and adaptive weighting process.

4.5. Comparison of Weighting Methods

The weighting methods offer distinct approaches to dynamically adjusting the contributions of loss functions during model training. The variance-based weighting method emphasizes loss functions exhibiting higher variability in performance under the assumption that increased variance indicates a more dynamic or complex contribution to the optimization process. Loss functions with greater variability are considered to encapsulate more challenging aspects of the task, thus requiring additional attention during training. By adaptively increasing the weights of these high-variance functions, the model shifts its focus toward aspects of the task that may otherwise hinder convergence, thereby promoting a more balanced and efficient optimization.

In contrast, the MAD-based weighting method prioritizes stability by assigning higher weights to loss functions with smaller deviations from their median, signifying more consistent performance over time. This method is designed to enhance robustness to outliers, ensuring that stable loss functions are emphasized while mitigating the impact of abrupt fluctuations. By reducing the likelihood of the model overreacting to transient changes, MAD-based weighting supports a more stable and reliable training process, safeguarding against destabilization.

The Bayesian-based weighting method integrates both prior knowledge and real-time data to update loss function weights dynamically. By assessing the likelihood of each loss function's contribution to the overall performance, this method allows the model to combine predefined expectations, such as the relative importance of certain tasks, with observed performance data. This results in a more informed and adaptive training strategy, where the model balances accumulated learning with prior criteria, leading to a more refined and targeted optimization process.

4.6. Normalization of Loss Histories

To ensure that the weighting mechanism is fair and unaffected by the scale of individual loss values, we apply normalization techniques to the loss histories \mathcal{H}_i before computing statistical measures. Two primary normalization methods are used: min-max scaling and symmetric log scaling.

Min-Max Scaling. Min-max scaling normalizes the loss history \mathcal{H}_i of each loss function to a fixed range, typically between 0 and 1. This scaling is crucial to prevent loss functions with larger absolute values from dominating the weighting process. The min-max scaling is defined as:

$$\mathcal{H}_i^{scaled} = \frac{\mathcal{H}_i - \min(\mathcal{H}_i)}{\max(\mathcal{H}_i) - \min(\mathcal{H}_i)} \quad (9)$$

where $\min(\mathcal{H}_i)$ and $\max(\mathcal{H}_i)$ are the minimum and maximum values of the loss history for the i -th loss function. This method ensures that all loss functions contribute equally, regardless of their original scale.

Symmetric Log Scaling. While min-max scaling addresses the scale issue, it does not handle cases where the distribution of loss values is skewed. Symmetric log scaling is applied to better handle such skewness, particularly when loss values span several orders of magnitude or contain both positive and negative values. The symmetric log scaling function is defined as:

$$\mathcal{H}_i^{\text{log-scaled}} = \begin{cases} \log(1 + \mathcal{H}_i), & \text{if } \mathcal{H}_i \geq 0 \\ -\log(1 - \mathcal{H}_i), & \text{if } \mathcal{H}_i < 0 \end{cases} \quad (10)$$

By compressing the range of loss values, symmetric log scaling minimizes the impact of outliers, ensuring that variance and MAD calculations become more resilient and accurately reflect the overall behavior of the loss function.

Consequently, we first apply symmetric log normalization to stabilize the data distribution and then use min-max normalization to rescale the values within the range of 0 to 1. By first stabilizing the data with symmetric log scaling and then normalizing the range with min-max scaling, the process ensures that both the distribution and scale of the loss values are handled appropriately, leading to more robust and effective weight adjustments during training.

4.7. Adaptive Weighting and the Challenges of Unbounded Weighting

In the DMF framework, the weights assigned to multiple loss functions are typically constrained to sum to 1. This ensures that the contributions of each loss function are proportionally balanced and normalized, preventing any single component from disproportionately affecting the optimization process. This approach is standard in multi-loss function optimization, as it promotes balanced optimization and reduces the risk of overemphasizing any particular loss function.

Without this constraint, however, several challenges can arise. First, unbounded growth in certain weights may occur, allowing specific components to dominate the optimization and potentially leading to the neglect of other vital tasks. This imbalance can distort the learning process, resulting in suboptimal performance across the model’s objectives. Additionally, unconstrained weights may introduce instability into the optimization process, as the overemphasis on certain loss functions can cause erratic gradients, oscillating performance, and difficulties in reaching convergence. Delayed convergence is another potential issue, as the model may frequently shift focus between tasks, prolonging the training process and hindering the achievement of a stable solution. These risks emphasize the importance of maintaining the weight sum constraint to ensure stable and efficient training.

5. Evaluation Metrics

To evaluate the performance of our method, we use a range of standard metrics, including dice, intersection over union (IoU), precision, recall, and f1-score. These metrics comprehensively assess the model’s ability to segment and classify pixels correctly. The dice score measures the similarity between predicted and ground

truth segments, emphasizing precision and recall. IoU evaluates the overlap between the predicted and actual segments, providing insight into how well the prediction captures the object. Precision quantifies how many of the predicted positives are true, while accuracy measures the overall correctness of the predictions, considering both positive and negative classifications. Together, these metrics offer a detailed view of model performance across multiple aspects of segmentation and classification.

$$Dice = \frac{2 \times TP}{2 \times TP + FP + FN} \quad (11)$$

$$IoU = \frac{TP}{TP + FP + FN} \quad (12)$$

$$Precision = \frac{TP}{TP + FP} \quad (13)$$

$$Recall = \frac{TP}{TP + FN} \quad (14)$$

$$F1\text{-score} = \frac{2 \times Precision \times Recall}{Precision + Recall} \quad (15)$$

where TP represents the number of true positives, correctly predicted pixels in the positive class; TN is the number of true negatives, correctly predicted pixels in the negative class; FP refers to false positives, or incorrectly predicted positive pixels; and FN denotes false negatives, where pixels that should have been predicted as positive were missed.

6. Loss Functions

In semantic segmentation tasks, loss functions are crucial in guiding the optimization process. Different loss functions minimize the error between the predicted segmentation and the ground truth. For our model, we use several loss functions, including categorical cross-entropy, mean intersection over union (mean IoU), mean dice loss, Focal loss, and Tversky loss, each designed to optimize different aspects of segmentation performance.

6.1. Categorical cross-entropy

Categorical cross-entropy is a widely used loss function in multi-class segmentation tasks. It measures the dissimilarity between the predicted class probabilities and the true class distribution. For a set of C classes, the categorical cross-entropy loss is defined as:

$$\mathcal{L}_{CE} = -\frac{1}{N} \sum_{i=1}^N \sum_{c=1}^C y_{ic} \log(\hat{y}_{ic}) \quad (16)$$

where N is the number of pixels, C is the number of classes, y_{ic} is the ground truth probability that pixel i belongs to class c , and \hat{y}_{ic} is the predicted probability for pixel i in class c .

6.2. Mean Intersection over Union (Mean IoU)

Mean IoU is used to evaluate the overlap between the predicted segmentation and the ground truth. It is also a loss function by optimizing the average IoU over all classes. Mean IoU is computed as:

$$\mathcal{L}_{IoU} = 1 - \frac{1}{C} \sum_{c=1}^C \frac{TP_c}{TP_c + FP_c + FN_c} \quad (17)$$

where TP_c , FP_c , and FN_c represent the true positives, false positives, and false negatives for class c , respectively, and C is the number of classes.

6.3. Mean Dice Loss

The mean dice loss is derived from the dice similarity coefficient and is widely used to measure overlap between two sets. For segmentation, it can be adapted as a loss function to optimize the dice score for all classes:

$$\mathcal{L}_{Dice} = 1 - \frac{1}{C} \sum_{c=1}^C \frac{2 \times TP_c}{2 \times TP_c + FP_c + FN_c} \quad (18)$$

where TP_c , FP_c , and FN_c correspond to the true positives, false positives, and false negatives for class c , and C represents the number of classes.

6.4. Focal Loss

Focal loss addresses class imbalance by assigning more weight to hard-to-classify examples, reducing the contribution of easy examples. It modifies the cross-entropy loss with a modulating factor:

$$\mathcal{L}_{Focal} = -\frac{1}{N} \sum_{i=1}^N \sum_{c=1}^C \alpha_c (1 - \hat{y}_{ic})^\gamma y_{ic} \log(\hat{y}_{ic}) \quad (19)$$

where α_c is a balancing factor for class c , γ , is a focusing parameter that adjusts the rate at which easy examples are down-weighted, y_{ic} is the ground truth, and \hat{y}_{ic} is the predicted probability.

6.5. Tversky Loss

Tversky loss is a generalization of dice loss that allows for a tunable trade-off between false positives and false negatives. It is advantageous when there is a significant class imbalance. The Tversky loss is defined as:

$$\mathcal{L}_{Tversky} = 1 - \frac{1}{C} \sum_{c=1}^C \frac{TP_c}{TP_c + \alpha \cdot FP_c + \beta \cdot FN_c} \quad (20)$$

where α and β are hyperparameters that control the penalty for false positives and false negatives, respectively. This formulation allows the model to be more sensitive to either false positives or false negatives based on the specific task requirements.

7. Class Balanced Dice Loss

Class imbalance is a common issue in semantic segmentation tasks. Certain classes (e.g., the background) may dominate the image, resulting in biased predictions. To address this, we propose the class-balanced dice (CB-Dice) loss, an extension of the standard dice loss that incorporates class weights based on the pixel distribution across classes.

The CB-Dice loss is motivated by the need to give more importance to minority classes, often underrepresented in the data. In our implementation, we first calculate the class weights by determining the proportion of pixels that belong to each class. The intuition behind this is that the higher the proportion of a class in the image, the lower its weight should be avoided by biasing the model towards the majority class. These class weights are computed as follows:

$$\text{class ratio} = \frac{P_i}{P} \quad (21)$$

$$w_i = \frac{(\text{class ratio})^{-1}}{\sum_i (\text{class ratio})^{-1}} \quad (22)$$

where P_i represents the number of pixels belonging to class i , and P is the total number of pixels in the image. By subtracting the class ratio from 1, we ensure that classes with fewer pixels receive higher weights, balancing the impact of majority and minority classes on the final loss value. The core of the CB-Dice loss is computed similarly to the traditional dice score but includes class weights. The dice score for each class is computed using the true positives (TP), false positives (FP), and false negatives (FN), as follows:

$$Dice_i = \frac{2 \cdot TP_i}{2 \cdot TP_i + FP_i + FN_i} \quad (23)$$

The final CB-Dice score is the weighted sum of the individual dice score:

$$CB\text{-Dice} = \sum_i w_i \cdot Dice_i \quad (24)$$

The corresponding CB-Dice loss is defined as:

$$\mathcal{L}_{CB\text{-Dice}} = 1 - CB\text{-Dice} \quad (25)$$

The CB-Dice loss ensures that the optimization process seeks to maximize the CB-Dice score, thereby improving the segmentation performance across all classes, especially the minority ones. This approach leads to a more balanced learning process and helps to mitigate the effects of class imbalance in segmentation tasks.

8. Dataset and Materials

While deep learning classification tasks tend to be less complex and generally involve a single loss function, more challenging tasks often require multiple loss functions to handle fine-grained predictions, boundary accuracy, and class imbalance. This makes them ideal for evaluating adaptive optimization frameworks like DMF. Segmentation tasks, which often involve multiple loss functions, provide a valuable context for testing the DMF framework’s effectiveness in addressing the complexities of these tasks. Therefore, our focus on these tasks enables a comprehensive assessment of DMF’s capabilities.

This research utilizes breast cancer segmentation as a case study to demonstrate the compatibility and applicability of the DMF framework. By employing the DMF framework, the model can dynamically adjust its focus between multiple cost functions throughout the training process, ensuring that each receives appropriate attention at the right time. To support this investigation, three primary breast ultrasound image segmentation datasets are utilized: the breast ultrasound images dataset, the breast ultrasound cancer dataset, and a third dataset featuring synthetic images generated from a generative model.

8.1. Breast Ultrasound Segmentation Images

The Breast Ultrasound Segmentation Images (BUSI) dataset was introduced by Al-Dhabyani et al. [29]. It was collected in 2018 at Baheya Hospital for Early Detection & Treatment of Women’s Cancer in Cairo, Egypt. It consists of data from 600 female patients aged 25 to 75 years. The dataset comprises 780 images categorized into normal, benign, and malignant groups. However, to evaluate the segmentation model in this research, only the benign and malignant categories were used, along with their corresponding ground truth masks.

8.2. Breast Ultrasound Cancer Dataset

Another dataset used in this research was introduced by Iqbal et al. [30], which is an annotated version of the Mendeley dataset [31], referred to as the Breast Ultrasound Cancer (BUSC) dataset. The original Mendeley dataset, consisting of ultrasound images of benign and malignant breast tumors, lacked detailed annotations. However, Iqbal et al. collaborated with experienced radiologists to manually annotate the images, providing ground truth for the segmentation task. The transformed version includes 100 benign and 150 malignant tumor images with annotations; both images and masks have a resolution of 128×128 pixels.

8.3. Breast Ultrasound Synthetic Dataset

Additionally, this research incorporated 500 synthetic images of breast tumors created by training a generative model on unannotated breast ultrasound images, referred to as the BUS Synthetic Dataset (BUS), as proposed by Iqbal et al. [30]. The corresponding probability maps for these synthetic images were generated through a separate model designed to produce segmentation probability outputs. Both the

images and masks have a resolution of 128×128 pixels, contributing to a more comprehensive and effective training dataset.

9. Preprocessing with Bilateral Filtering

In this research, bilateral filtering was applied during the preprocessing stage to reduce speckle noise in breast ultrasound images. The bilateral filter is particularly useful because it smooths the image while preserving edges, critical for distinguishing between benign and malignant regions in the segmentation task. Studies like [32] show that speckle-reducing bilateral filtering (SRBF) enhances boundaries while preserving features, making it useful for ultrasound imaging and segmentation. The bilateral filter combines both spatial proximity and pixel intensity in its weighting function. The filtered image $I_f(x)$ is computed as:

$$I_f(x) = \frac{1}{W_p} \sum_{x_i \in \Omega} I(x_i) \cdot \exp\left(-\frac{|x - x_i|^2}{2\sigma_s^2}\right) \cdot \exp\left(-\frac{|I(x) - I(x_i)|^2}{2\sigma_r^2}\right) \quad (26)$$

where $I(x)$ is the intensity of the pixel at location x , $I(x_i)$ is the intensity of the neighboring pixel x_i , and Ω represents the neighborhood around x . The parameter σ_s controls the spatial proximity weight, determining how much influence nearby pixels have, while σ_r controls the intensity difference weight, favoring pixels with similar intensity values. W_p is the normalization factor, which is calculated as:

$$W_p = \sum_{x_i \in \Omega} \exp\left(-\frac{|x - x_i|^2}{2\sigma_s^2}\right) \cdot \exp\left(-\frac{|I(x) - I(x_i)|^2}{2\sigma_r^2}\right) \quad (27)$$

This filter effectively reduces speckle noise while preserving the boundaries in ultrasound images.

10. Results

This section presents the results of applying the DMF framework with different auxiliary loss functions. Each experiment involved training models using three different weighting methods: variance-based, MAD-based, and Bayesian-based. To maintain fairness in comparisons, we utilized a basic U-Net model across all experiments to ensure that the methods, rather than model architectures, are being compared. While more advanced models could enhance performance, our goal is to isolate the benefits of the DMF framework itself. For every method, ten experiments were conducted with the same weight initialization and data distribution for each experiment, where 70% of the data was used for training, 15% for validation, and 15% for testing, ensuring consistent comparison. The evaluation metrics include dice, IoU, f1-score, precision, recall, and CB-Dice. The loss functions used in each experiment comprised categorical cross-entropy, mean IoU, and mean Dice as primary loss functions; additionally, Tversky, Focal, and CB-Dice were utilized as auxiliary loss functions. The demo source code for implementing the proposed methodology

is openly available on GitHub at <https://github.com/amingolnari/Demo-Dynamic-Memory-Fusion-Framework>. To facilitate usage, readers can run the code directly in Google Colab.

Table 1 compares model performance, reported in percentages, with and without the DMF framework, and various loss functions on the BUSI dataset. Similarly, Table 2 compares model performance on the BUSC dataset using the same reporting style. Additionally, Table 3 compares model performance on the BUS dataset.

Table 1: Performance metrics summary using the DMF framework with different auxiliary loss functions, alongside a baseline model without DMF. All models were evaluated on the BUSI dataset.

| Loss Function | Weighting Method | Dice | IoU | F1-score | Precision | Recall | CB-Dice |
|---------------------|------------------|------------------------------------|------------------------------------|------------------------------------|------------------------------------|------------------------------------|------------------------------------|
| Tversky Loss | Variance | 93.30 \pm 0.91 | 87.91 \pm 1.44 | 93.36 \pm 0.92 | 94.37 \pm 1.02 | 92.28 \pm 1.46 | 89.36 \pm 1.76 |
| | MAD | 93.75 \pm 0.69 | 88.64 \pm 1.12 | 93.82 \pm 0.68 | 95.31 \pm 0.70 | 92.38 \pm 1.07 | 90.17 \pm 1.37 |
| | Bayesian | 90.53 \pm 1.56 | 83.57 \pm 2.31 | 90.67 \pm 1.73 | 92.17 \pm 3.82 | 89.38 \pm 0.76 | 85.01 \pm 3.04 |
| Focal Loss | Variance | 94.35 \pm 1.01 | 89.67 \pm 1.70 | 94.43 \pm 0.97 | 96.12 \pm 0.61 | 92.84 \pm 1.71 | 91.13 \pm 1.68 |
| | MAD | 92.67 \pm 1.02 | 86.88 \pm 1.63 | 92.98 \pm 0.91 | 96.95 \pm 0.37 | 89.41 \pm 1.52 | 88.41 \pm 1.72 |
| | Bayesian | 93.19 \pm 1.17 | 87.75 \pm 1.86 | 93.22 \pm 1.18 | 94.13 \pm 1.12 | 92.42 \pm 1.44 | 89.25 \pm 2.27 |
| CB-Dice Loss | Variance | 95.22 \pm 0.53 | 91.34 \pm 0.43 | 95.25 \pm 0.55 | 95.58 \pm 0.89 | 94.93 \pm 0.87 | 92.55 \pm 0.97 |
| | MAD | 95.02 \pm 0.52 | 90.75 \pm 0.49 | 94.98 \pm 0.49 | 95.14 \pm 0.39 | 94.82 \pm 0.51 | 91.98 \pm 0.76 |
| | Bayesian | 92.60 \pm 0.46 | 87.42 \pm 0.30 | 93.31 \pm 0.53 | 91.56 \pm 0.18 | 95.12 \pm 0.87 | 88.94 \pm 0.32 |
| No Auxiliary Loss | Variance | 93.93 \pm 1.08 | 88.99 \pm 1.77 | 93.98 \pm 1.05 | 95.31 \pm 0.63 | 92.72 \pm 1.70 | 90.22 \pm 1.87 |
| | MAD | 93.20 \pm 0.95 | 87.77 \pm 1.55 | 93.32 \pm 0.88 | 95.34 \pm 1.20 | 91.45 \pm 1.93 | 89.05 \pm 1.55 |
| | Bayesian | 91.97 \pm 1.05 | 85.51 \pm 1.64 | 91.98 \pm 1.06 | 92.03 \pm 1.60 | 91.99 \pm 0.67 | 87.09 \pm 1.85 |
| Using Fixed Weights | Not Used | 91.84 \pm 0.73 | 85.19 \pm 0.97 | 91.81 \pm 0.86 | 92.78 \pm 0.96 | 90.85 \pm 0.63 | 87.05 \pm 1.41 |

The findings from Table 1 highlight that using the CB-Dice loss function with the variance-based weighting method consistently produced the best results across most metrics, including dice ($95.22 \pm 0.53\%$), IoU ($91.34 \pm 0.43\%$), f1-score ($95.25 \pm 0.55\%$), and CB-Dice ($92.55 \pm 0.97\%$). This combination outperformed other loss functions and weighting methods. Models utilizing the Focal and Tversky losses also showed strong performance, particularly when combined with the variance-based and MAD-based weighting methods. Focal loss achieved the highest precision ($96.12 \pm 0.61\%$) among all setups. In contrast, models without auxiliary loss or using fixed weights performed noticeably worse, particularly with lower IoU and CB-Dice scores.

The comparison of model predictions with different auxiliary loss functions and the ground truth masks is presented in Figure 1, showcasing the segmentation performance across multiple samples from the BUSI dataset. Each model was selected based on its highest score on the CB-Dice metric.

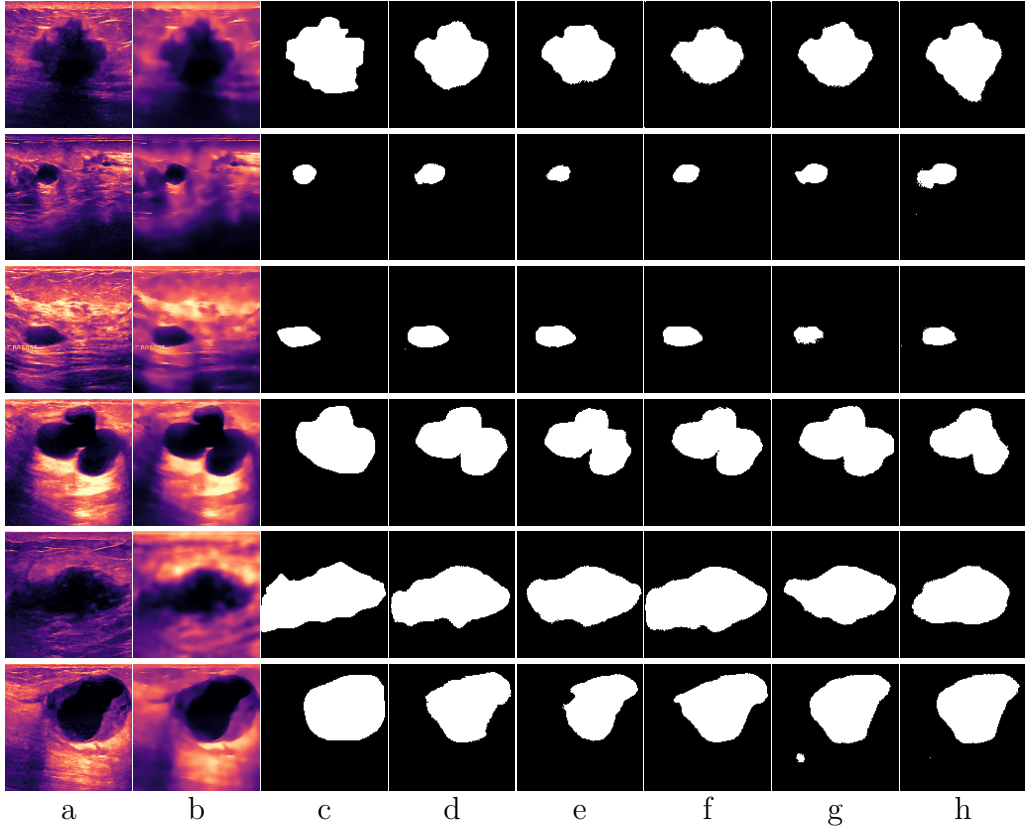


Figure 1: Each row presents a sample from the BUSI dataset, showing the input breast ultrasound image and the corresponding ground truth mask alongside model predictions. (a) Original breast ultrasound image, (b) Bilaterally filtered image, (c) Ground truth mask, (d) Predicted mask using DMF with Tversky loss as the auxiliary loss function, (e) Predicted mask using DMF with Focal loss as the auxiliary loss function, (f) Predicted mask using DMF with CB-Dice loss as the auxiliary loss function, (g) Predicted mask using DMF without auxiliary loss function, (h) Predicted mask using fixed weights for loss functions.

Table 2: Performance metrics summary using the DMF framework with different auxiliary loss functions, alongside a baseline model without DMF. All models were evaluated on the BUSC dataset.

| Loss Function | Weighting Method | Dice | IoU | F1-score | Precision | Recall | CB-Dice |
|---------------------|------------------|---------------------|---------------------|---------------------|---------------------|---------------------|---------------------|
| Tversky Loss | Variance | 95.29 ± 0.31 | 91.15 ± 0.52 | 95.34 ± 0.25 | 94.27 ± 0.63 | 96.45 ± 0.16 | 93.68 ± 0.44 |
| | MAD | 94.79 ± 0.69 | 90.35 ± 1.13 | 94.85 ± 0.65 | 94.36 ± 1.31 | 95.41 ± 1.59 | 92.93 ± 0.90 |
| | Bayesian | 94.94 ± 0.43 | 90.59 ± 0.67 | 94.98 ± 0.40 | 94.97 ± 0.86 | 95.04 ± 1.55 | 92.66 ± 1.17 |
| Focal Loss | Variance | 94.67 ± 0.23 | 90.07 ± 0.37 | 94.80 ± 0.21 | 92.90 ± 0.54 | 96.78 ± 0.21 | 92.70 ± 0.66 |
| | MAD | 94.80 ± 0.41 | 90.21 ± 0.71 | 94.87 ± 0.43 | 93.64 ± 0.66 | 96.17 ± 1.21 | 92.67 ± 0.73 |
| | Bayesian | 94.75 ± 0.62 | 90.24 ± 1.09 | 94.76 ± 0.61 | 95.07 ± 0.56 | 94.45 ± 0.72 | 92.63 ± 0.82 |
| CB-Dice Loss | Variance | 95.28 ± 0.53 | 91.75 ± 0.32 | 95.67 ± 0.22 | 94.44 ± 0.41 | 96.94 ± 0.85 | 93.28 ± 0.71 |
| | MAD | 94.49 ± 0.25 | 89.75 ± 0.41 | 94.53 ± 0.30 | 94.28 ± 0.64 | 94.80 ± 1.21 | 92.51 ± 0.68 |
| | Bayesian | 95.24 ± 0.24 | 91.07 ± 0.39 | 95.27 ± 0.22 | 94.43 ± 0.68 | 96.14 ± 0.27 | 93.55 ± 0.63 |
| No Auxiliary Loss | Variance | 94.89 ± 0.90 | 89.10 ± 1.50 | 94.01 ± 0.74 | 94.28 ± 0.78 | 93.76 ± 1.03 | 92.63 ± 0.90 |
| | MAD | 93.95 ± 1.15 | 89.31 ± 0.74 | 93.55 ± 0.96 | 93.64 ± 1.04 | 93.47 ± 1.32 | 92.21 ± 1.55 |
| | Bayesian | 94.37 ± 0.64 | 90.51 ± 0.32 | 94.40 ± 0.50 | 93.83 ± 0.70 | 94.98 ± 0.54 | 92.48 ± 0.89 |
| Using Fixed Weights | Not Used | 93.40 ± 0.81 | 89.77 ± 1.14 | 94.06 ± 0.89 | 93.76 ± 1.41 | 94.36 ± 0.78 | 92.39 ± 1.08 |

Table 2 presents that the dice scores range from 93.95% to 95.29%, while the IoU values vary between 89.10% and 91.75%, reflecting minimal variation between methods. Notably, the CB-Dice loss function with the Variance-based weighting method achieved the highest mean IoU ($91.75 \pm 0.32\%$) and nearly the highest dice score ($95.28 \pm 0.53\%$), demonstrating superior overall performance. Meanwhile, Tversky loss with variance-based weighting performed similarly well, achieving the highest dice score ($95.29 \pm 0.31\%$) and a recall of ($96.45 \pm 0.16\%$). The models without auxiliary losses showed slightly lower metrics, with the best dice score ($94.89 \pm 0.90\%$) using the variance-based weighting method. These results indicate that, while subtle, the choice of auxiliary loss function and weighting method has only a minor impact on overall model performance in this dataset.

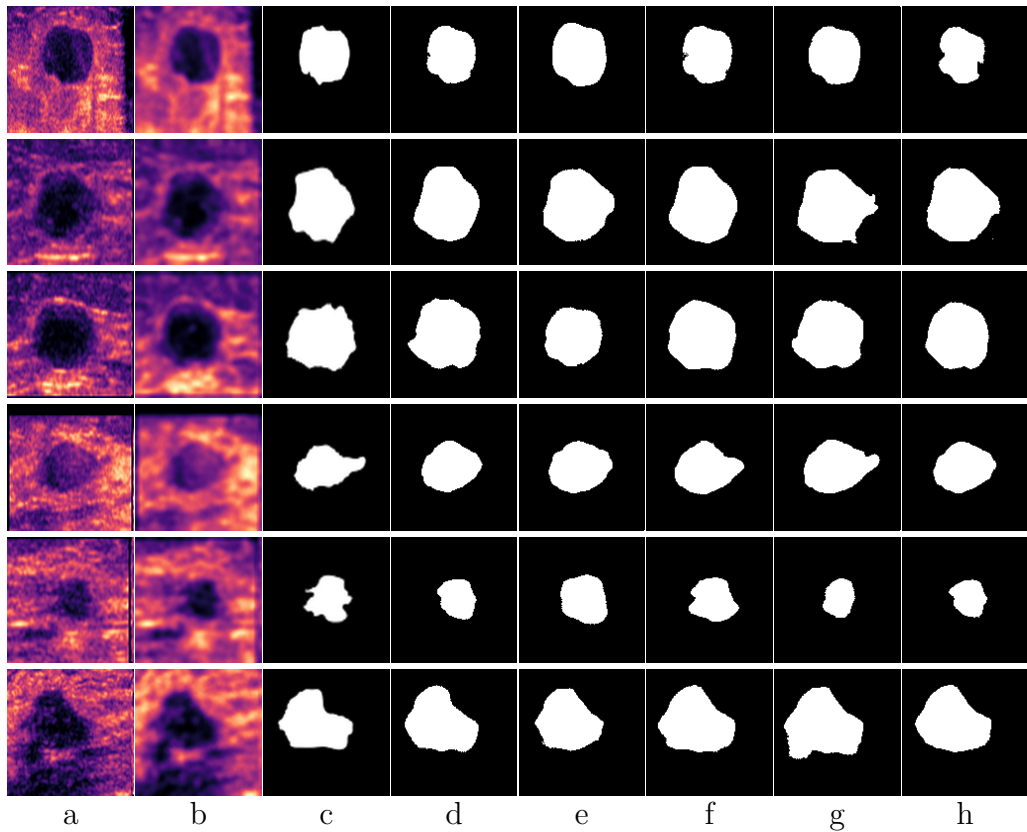


Figure 2: Each row presents a sample from the BUSC dataset, showing the input breast ultrasound image and the corresponding ground truth mask alongside model predictions. (a) Original breast ultrasound image, (b) Bilaterally filtered image, (c) Ground truth mask, (d) Predicted mask using DMF with Tversky loss as the auxiliary loss function, (e) Predicted mask using DMF with Focal loss as the auxiliary loss function, (f) Predicted mask using DMF with CB-Dice loss as the auxiliary loss function, (g) Predicted mask using DMF without auxiliary loss function, (h) Predicted mask using fixed weights for loss functions.

The comparison of model predictions with different auxiliary loss functions and the ground truth masks is presented in Figure 2, showcasing the segmentation per-

formance across multiple samples from the BUSC dataset. Each model was selected based on its highest score on the CB-Dice metric.

Table 3: Performance metrics summary using the DMF framework with different auxiliary loss functions, alongside a baseline model without DMF. All models were evaluated on the BUS dataset.

| Loss Function | Weighting Method | Dice | IoU | F1-score | Precision | Recall | CB-Dice |
|---------------------|------------------|------------------------------------|------------------------------------|------------------------------------|------------------------------------|------------------------------------|------------------------------------|
| Tversky Loss | Variance | 93.35 \pm 0.22 | 91.28 \pm 0.37 | 95.42 \pm 0.21 | 97.21 \pm 0.42 | 93.69 \pm 0.49 | 93.20 \pm 0.30 |
| | MAD | 92.34 \pm 0.45 | 86.27 \pm 0.27 | 92.78 \pm 0.39 | 97.33 \pm 0.27 | 88.86 \pm 0.64 | 88.72 \pm 0.65 |
| | Bayesian | 94.15 \pm 0.32 | 89.24 \pm 0.59 | 94.20 \pm 0.34 | 95.53 \pm 0.58 | 93.14 \pm 0.68 | 91.47 \pm 0.49 |
| Focal Loss | Variance | 94.08 \pm 0.54 | 89.14 \pm 0.92 | 94.24 \pm 0.51 | 96.81 \pm 0.28 | 91.81 \pm 0.76 | 91.33 \pm 0.79 |
| | MAD | 93.09 \pm 0.18 | 87.43 \pm 0.29 | 93.37 \pm 0.15 | 96.97 \pm 0.17 | 90.07 \pm 0.29 | 89.80 \pm 0.25 |
| | Bayesian | 94.27 \pm 1.31 | 89.47 \pm 1.67 | 94.37 \pm 0.96 | 95.80 \pm 0.32 | 92.98 \pm 1.93 | 91.62 \pm 1.48 |
| CB-Dice Loss | Variance | 95.71 \pm 0.37 | 91.90 \pm 0.63 | 95.79 \pm 0.35 | 95.30 \pm 0.71 | 95.68 \pm 0.62 | 93.72 \pm 0.67 |
| | MAD | 95.05 \pm 0.75 | 91.54 \pm 0.46 | 95.27 \pm 0.63 | 93.30 \pm 0.53 | 97.31 \pm 0.84 | 93.65 \pm 0.38 |
| | Bayesian | 92.79 \pm 0.51 | 87.19 \pm 0.81 | 93.32 \pm 0.41 | 90.16 \pm 0.87 | 96.28 \pm 0.23 | 89.55 \pm 0.80 |
| No Auxiliary Loss | Variance | 93.99 \pm 0.36 | 88.96 \pm 0.62 | 94.11 \pm 0.35 | 96.24 \pm 0.30 | 92.06 \pm 0.48 | 91.20 \pm 0.55 |
| | MAD | 93.26 \pm 1.58 | 87.81 \pm 2.58 | 93.57 \pm 1.34 | 96.94 \pm 0.12 | 90.47 \pm 2.58 | 90.08 \pm 2.40 |
| | Bayesian | 93.84 \pm 0.11 | 88.70 \pm 0.19 | 93.93 \pm 0.12 | 95.80 \pm 0.63 | 92.16 \pm 0.50 | 90.99 \pm 0.15 |
| Using Fixed Weights | Not Used | 92.16 \pm 1.38 | 85.34 \pm 0.78 | 91.29 \pm 0.67 | 91.64 \pm 0.89 | 90.93 \pm 0.76 | 88.28 \pm 1.46 |

Notably, the Table 3 highlights that the CB-Dice loss with variance-based weighting outperformed all other configurations, achieving the highest dice score ($95.71 \pm 0.37\%$), IoU ($91.90 \pm 0.63\%$), f1-score ($95.79 \pm 0.35\%$), and CB-Dice ($93.72 \pm 0.67\%$), making it the most effective combination. The MAD-based weighting method with CB-Dice loss also showed strong results, particularly in precision ($97.31 \pm 0.84\%$). Among the models using Tversky loss, the MAD-based weighting method excelled in precision ($97.33 \pm 0.27\%$) and provided a balanced performance across metrics. Meanwhile, models without auxiliary loss had consistently lower results, with the highest dice score of ($91.20 \pm 0.55\%$) and IoU of ($88.96 \pm 0.62\%$), falling short compared to models with auxiliary losses.

The comparison of model predictions with different auxiliary loss functions and the ground truth masks is presented in Figure 3, showcasing the segmentation performance across multiple samples from the BUS dataset. Each model was selected based on its highest score on the CB-Dice metric.

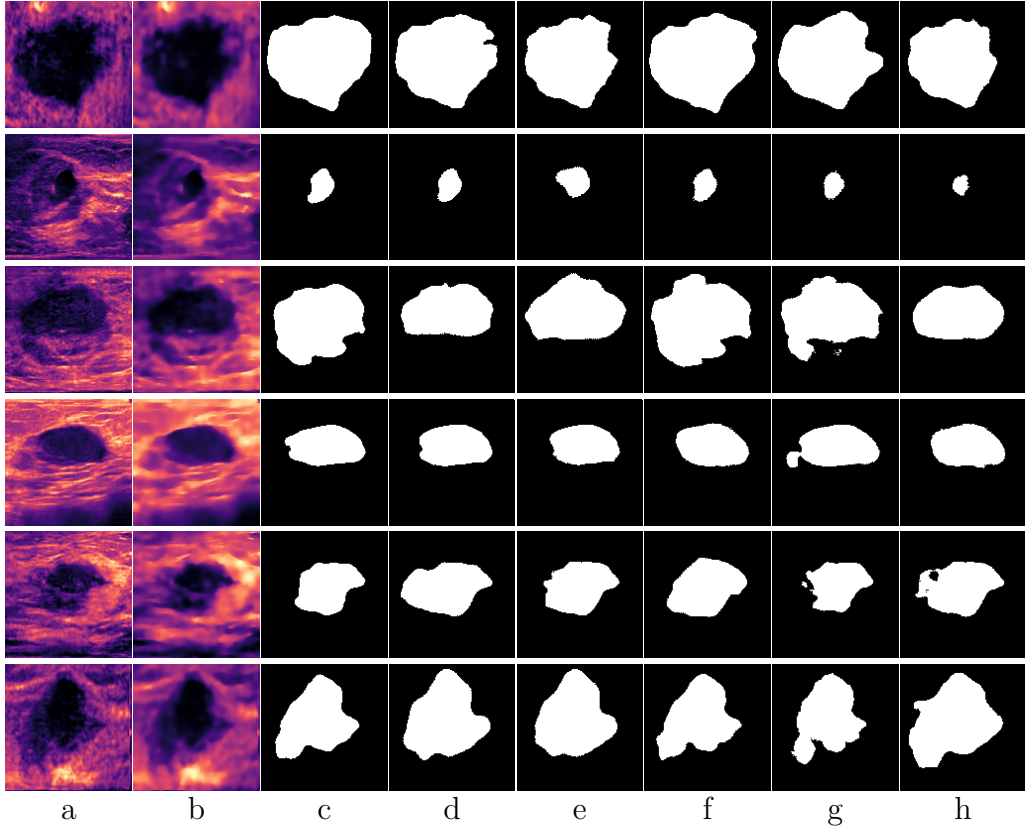


Figure 3: Each row presents a sample from the BUS dataset, showing the input breast ultrasound image and the corresponding ground truth mask alongside model predictions. (a) Original breast ultrasound image, (b) Bilaterally filtered image, (c) Ground truth mask, (d) Predicted mask using DMF with Tversky loss as the auxiliary loss function, (e) Predicted mask using DMF with Focal loss as the auxiliary loss function, (f) Predicted mask using DMF with CB-Dice loss as the auxiliary loss function, (g) Predicted mask using DMF without auxiliary loss function, (h) Predicted mask using fixed weights for loss functions.

Overall, these results demonstrate that the choice of auxiliary loss function and the weighting method play critical roles in optimizing segmentation performance on each dataset.

Figure 4 shows the dynamic weighting behavior of W_1 , W_2 , and W_3 during training for categorical cross-entropy, mean IoU, and mean dice loss functions in the DMF framework. It employs three different weighting methods: variance-based, MAD-based, and Bayesian-based. The variance-based method adjusts weights gradually in the early stages, responding to fluctuations in task performance while maintaining a balanced distribution throughout the training process. In contrast, the MAD-based method is more sensitive, resulting in sharper weight adjustments. Although the Bayesian-based method exhibits smooth changes, it adopts a more aggressive approach, focusing on a dominant task during training and maintaining this preference. Each technique offers a unique strategy for handling multi-task loss functions, with different levels of adaptability and task prioritization.

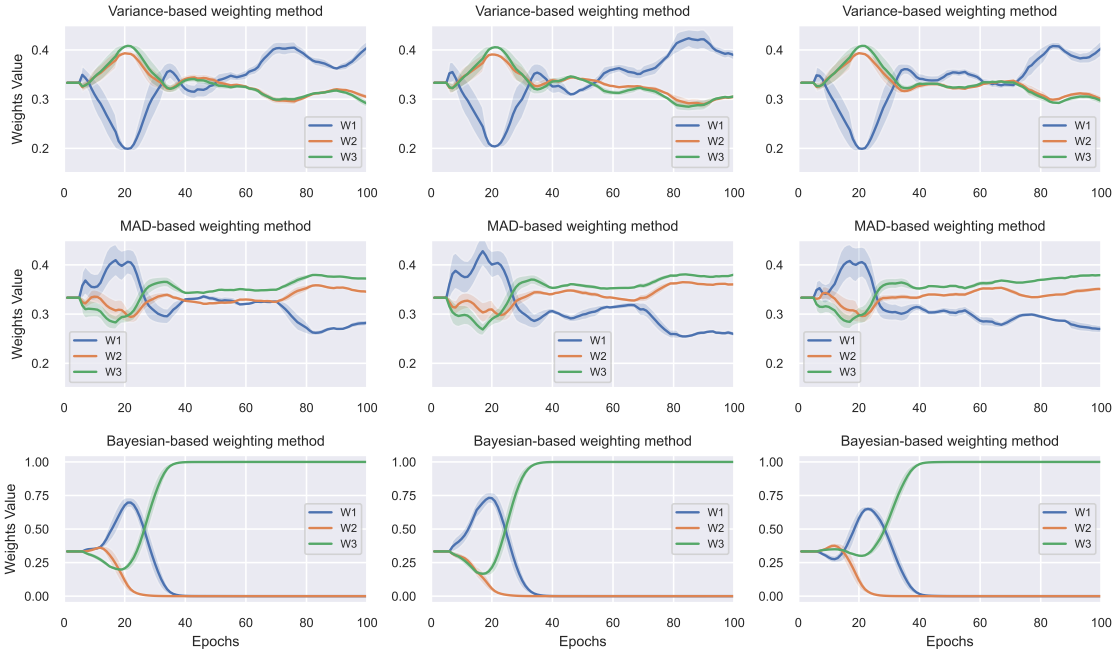


Figure 4: Weight dynamics of W1 in blue for categorical cross-entropy, W2 in red for mean IoU, and W3 in green for mean dice during training in the DMF framework. The first row shows the variance-based method, the second row shows the MAD-based method, and the third row shows the Bayesian-based method. Models are trained on the BUSI dataset

Figure 5 illustrates the dynamic behavior of the loss functions L1, L2, and L3, respectively, representing categorical cross-entropy, mean IoU, and mean Dice functions within the DMF framework. The figure demonstrates the performance of three different weighting methods: variance-based, MAD-based, and Bayesian-based. The convergence of all loss functions is evident as each steadily decreases without significant fluctuations.

After a certain number of epochs, there are no considerable changes in the loss values, indicating that they have reached a stable point. This confirms successful optimization convergence, where further training brings minimal improvements. Although the loss values remain stable, the weights continue to adjust (except for the Bayesian-based weighting method, which is aggressive yet smooth in its changes), according to Figure 4. This behavior suggests that the DMF framework avoids local minima and maintains adaptability during training, ensuring robust performance across tasks even in later stages.

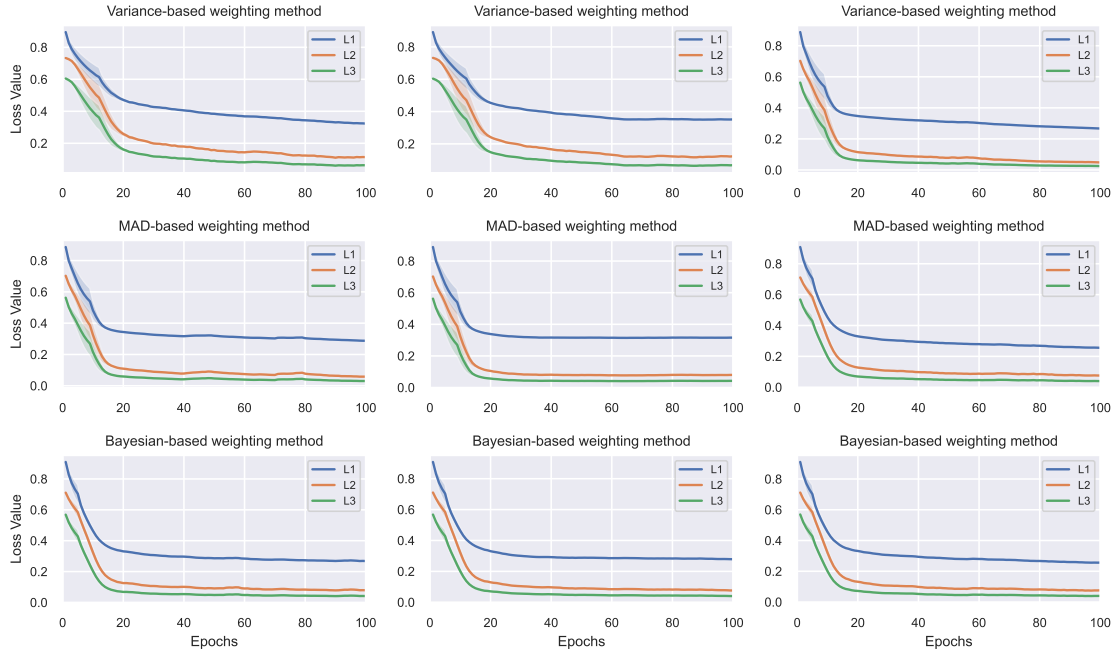


Figure 5: Loss dynamics of L1 in blue for categorical cross-entropy, L2 in red for mean IoU, and L3 in green for mean Dice during training in the DMF framework. The first row shows the variance-based method, the second row shows the MAD-based method, and the third row shows the Bayesian-based method. Models are trained on the BUSI dataset

11. Conclusion

In this study, we introduced the DMF framework for adaptive multi-loss function optimization in deep learning, specifically applied to breast cancer segmentation. The framework allows for real-time adjustment of loss function weights, effectively addressing challenges such as class imbalance and varying task importance during training.

Our experiments on the BUSI, BUSC, and BUS datasets demonstrated improvements in segmentation performance, supported by various evaluation metrics, including Dice, IoU, and Precision. The incorporation of CB-Dice loss has shown potential in mitigating class imbalance issues. The DMF framework is not limited to medical imaging and can be applied to other deep learning tasks requiring multiple loss functions. By providing open-source code, we aim to enhance reproducibility and encourage further exploration of this approach.

While deep learning classification tasks are generally less complex and typically involve only a single loss function, segmentation presents greater challenges. In segmentation, multiple loss functions are often necessary to address pixel-wise predictions, boundary accuracy, and class imbalance. This makes it a more suitable domain for testing adaptive optimization frameworks like DMF. Therefore, our focus on segmentation tasks allows us to fully explore and demonstrate the effectiveness

of the DMF framework in managing these complex tasks.

For future work, we suggest investigating the DMF framework’s scalability and its application in diverse machine learning scenarios. Previous observations may also be beneficial in limiting weight adjustments and exploring additional methods, such as exponential moving averages (EMA), for optimizing weight updates.

Data Availability Statement

The BUSI dataset can be accessed openly at <https://www.kaggle.com/datasets/sabahesaraki/breast-ultrasound-images-dataset>. The BUSC dataset is available at <https://data.mendeley.com/datasets/vckdnhtw26/1>, while the BUS Synthetic dataset can be found at <https://data.mendeley.com/datasets/r4phtn49r7/1>.

Declaration of Competing Interest

The authors declare that they have no known competing financial interests or personal relationships that could have appeared to influence the work reported in this paper.

Authorship Contribution Statement

Amin Golnari: Conceptualization, Software, Investigation, Methodology, Visualization, Writing – Original Draft, Writing – Review & Editing. **Mostafa Diba:** Investigation, Writing – Original Draft, Writing – Review & Editing.

Declaration of Generative AI in Scientific Writing

During the preparation of this work, the authors used OpenAI’s GPT-4o to enhance overall readability, improve language, and correct grammatical errors. After using this service, the authors reviewed and edited the content as needed and take full responsibility for the content of the publication.

References

- [1] J. Feng, X. Dong, S. Chen, L. Zhou, X. Zheng, Gbe-net: Global boundary enhancement network for breast lesion segmentation in ultrasound images, *Biomedical Signal Processing and Control* 96 (2024) 106644.
- [2] R. Wu, X. Lu, Z. Yao, Y. Ma, Mfmsnet: A multi-frequency and multi-scale interactive cnn-transformer hybrid network for breast ultrasound image segmentation, *Computers in Biology and Medicine* 177 (2024) 108616.
- [3] A. A. Heydari, C. A. Thompson, A. Mehmood, Softadapt: Techniques for adaptive loss weighting of neural networks with multi-part loss functions, *arXiv preprint arXiv:1912.12355* (2019).

- [4] K. R. M. Fernando, C. P. Tsokos, Dynamically weighted balanced loss: class imbalanced learning and confidence calibration of deep neural networks, *IEEE Transactions on Neural Networks and Learning Systems* 33 (7) (2021) 2940–2951.
- [5] B. Guermazi, R. Ksantini, N. Khan, A dynamically weighted loss function for unsupervised image segmentation, in: 2022 IEEE Eighth International Conference on Multimedia Big Data (BigMM), IEEE, 2022, pp. 73–78.
- [6] Y. Song, J. Y.-C. Teoh, K.-S. Choi, J. Qin, Dynamic loss weighting for multi-organ segmentation in medical images, *IEEE transactions on neural networks and learning systems* (2023).
- [7] A. Erdogan, E. Akagunduz, Fuseformer: A transformer for visual and thermal image fusion, *arXiv preprint arXiv:2402.00971* (2024).
- [8] Y. Zhao, Y. Xia, Y. Ding, Y. Liu, S. Liu, H. Wang, S2f-net: Shared-specific fusion network for infrared and visible image fusion, in: *Proceedings of the 2024 International Conference on Multimedia Retrieval*, 2024, pp. 497–505.
- [9] W.-F. Ou, L.-M. Po, C. Zhou, Y. A. U. Rehman, P.-F. Xian, Y.-J. Zhang, Fusion loss and inter-class data augmentation for deep finger vein feature learning, *Expert Systems with Applications* 171 (2021) 114584.
- [10] J. Tasnim, M. K. Hasan, Cam-qus guided self-tuning modular cnns with multi-loss functions for fully automated breast lesion classification in ultrasound images, *Physics in Medicine & Biology* 69 (1) (2023) 015018.
- [11] S. Jiang, J. Li, J. Zhang, Y. Wang, T. Xu, Dynamic loss for robust learning, *IEEE Transactions on Pattern Analysis and Machine Intelligence* (2023).
- [12] A. Jesson, T. Arbel, Brain tumor segmentation using a 3d fcn with multi-scale loss, in: *International MICCAI Brainlesion Workshop*, Springer, 2017, pp. 392–402.
- [13] M. Sharifzadeh, H. Benali, H. Rivaz, Phase aberration correction without reference data: An adaptive mixed loss deep learning approach, *arXiv preprint arXiv:2303.05747* (2023).
- [14] Q. Lv, R. Yang, Y. Chen, Z. Zhou, C. Zhang, S. Liu, Ssdfusion: A semantic segmentation driven framework for infrared and visible image fusion (2024).
- [15] Q. Gao, Q. Peng, S. Xuan, K. Xiong, Multi-loss function fusion for face recognition based on the convolutional neural network, in: *2019 12th International Congress on Image and Signal Processing, BioMedical Engineering and Informatics (CISP-BMEI)*, IEEE, 2019, pp. 1–6.

- [16] Y. Zhao, X. Shen, J. Chen, W. Qian, L. Sang, H. Ma, Learning active contour models based on self-attention for breast ultrasound image segmentation, *Biomedical Signal Processing and Control* 89 (2024) 105816.
- [17] Y. Zhao, X. Shen, J. Chen, W. Qian, H. Ma, L. Sang, loss for low-contrast medical image segmentation, *Machine Learning: Science and Technology* 5 (1) (2024) 015013.
- [18] F.-Y. Chao, L. Zhang, W. Hamidouche, O. Déforges, A multi-fov viewport-based visual saliency model using adaptive weighting losses for 360° images, *IEEE Transactions on Multimedia* 23 (2020) 1811–1826.
- [19] B. Sushma, A. Pulikala, Aapfc-busnet: Hierarchical encoder–decoder based cnn with attention aggregation pyramid feature clustering for breast ultrasound image lesion segmentation, *Biomedical Signal Processing and Control* 91 (2024) 105969.
- [20] C. Mang, A. Tahmasebimoradi, D. Danan, M. Yagoubi, A dynamic weighted loss function for enhancing the performance of neural networks, in: 16th World Congress on Computational Mechanics (WCCM), 2024.
- [21] S. Lu, F. Gao, C. Piao, Y. Ma, Dynamic weighted cross entropy for semantic segmentation with extremely imbalanced data, in: 2019 International conference on artificial intelligence and advanced manufacturing (AIAM), IEEE, 2019, pp. 230–233.
- [22] S. Maldonado, C. Vairetti, K. Jara, M. Carrasco, J. López, Owadapt: An adaptive loss function for deep learning using owa operators, *Knowledge-Based Systems* 280 (2023) 111022.
- [23] Y. Runda, X. Yan, Z. Mingfang, Z. Li, W. Hongbin, Lstm sentiment classification model based on one kind of dynamic loss weighting function, in: 2020 7th International Conference on Information Science and Control Engineering (ICISCE), IEEE, 2020, pp. 819–824.
- [24] D. Roy, R. Pramanik, R. Sarkar, Margin-aware adaptive-weighted-loss for deep learning based imbalanced data classification, *IEEE Transactions on Artificial Intelligence* 5 (2) (2023) 776–785.
- [25] R. Groenendijk, S. Karaoglu, T. Gevers, T. Mensink, Multi-loss weighting with coefficient of variations, in: Proceedings of the IEEE/CVF winter conference on applications of computer vision, 2021, pp. 1469–1478.
- [26] D. Ocampo, D. Posso, R. Namakian, W. Gao, Adaptive loss weighting for machine learning interatomic potentials, *Computational Materials Science* 244 (2024) 113155.

- [27] Z. Xiang, W. Peng, X. Liu, W. Yao, Self-adaptive loss balanced physics-informed neural networks, *Neurocomputing* 496 (2022) 11–34.
- [28] J. T. Barron, A general and adaptive robust loss function, in: *Proceedings of the IEEE/CVF conference on computer vision and pattern recognition*, 2019, pp. 4331–4339.
- [29] W. Al-Dhabyani, M. Gomaa, H. Khaled, A. Fahmy, Dataset of breast ultrasound images, *Data in brief* 28 (2020) 104863.
- [30] A. Iqbal, M. Sharif, Unet: A semi-supervised method for segmentation of breast tumor images using a u-shaped pyramid-dilated network, *Expert Systems with Applications* 221 (2023) 119718.
- [31] P. S. Rodrigues, Breast ultrasound image, *Mendeley Data* 1 (10) (2017).
- [32] S. Balocco, C. Gatta, O. Pujol, J. Mauri, P. Radeva, Srbf: Speckle reducing bilateral filtering, *Ultrasound in medicine & biology* 36 (8) (2010) 1353–1363.